Electronic Supplementary Material (ESI) for Energy & Environmental Science.
This journal is © The Royal Society of Chemistry 2015

Back-illuminated Si photocathode: a combined experimental and theoretical study for photocatalytic hydrogen evolution

Dowon Bae, [1] *Thomas Pedersen,* [2] *Brian Seger,* [1]*Mauro Malizia,*[1]*Andrej Kuznetsov,*[3]*Ole Hansen,* [2]*Ib Chorkendorff,* [1]*Peter C.K. Vesborg* [1†]

[1]Center for Individual Nanoparticle Functionality, Department of Physics, Technical University of Denmark, 2800 Kgs. Lyngby

[2]Department of Micro- and Nanotechnology, Technical University of Denmark, 2800 Kgs. Lyngby

[3]Centre for Materials Science and Nanotechnology, Department of Physics, University of Oslo, 0316 Oslo, Norway

Supplementary Information

1. Energy band diagrams of tandem PV assisted PEC system

A "buried junction" bottom cell design whose pn-junction is formed on the light incoming side can collect charge more efficiently, but the injection of electrons to the electrolyte can be hindered due to the upward band bending at the semiconductor/liquid interface (the bulk is now n-type). A sufficiently highly doped layer is required to minimize the thickness of the upward band bending region at the semiconductor/liquid interface so that injected electrons can tunnel through the interface. On the other hand, type I has an advantage over type II in easy injection of the collected charges by its shallow pn-junction at the semiconductor/liquid interface. And this pn-junction isolates the band-bending to within the photo-absorber. However, one cannot avoid charge collection losses due to the distant position of pn-junction from the light incident surface.

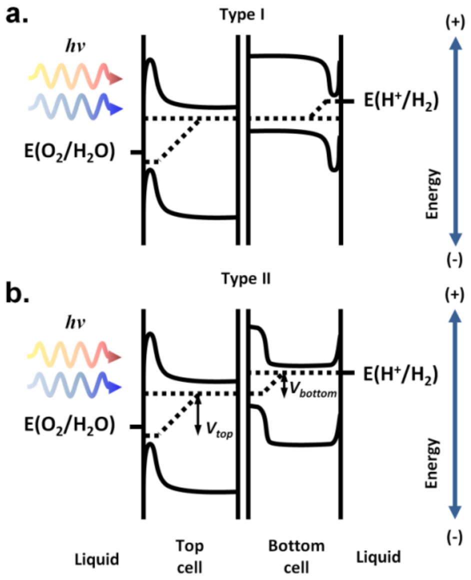

Figure S 1. Schematic energy band diagrams of tandem PV assisted PEC system for the configuration (a) with semiconductor/liquid junction (type I), and (b) the configuration (b) with buried junction (type II).

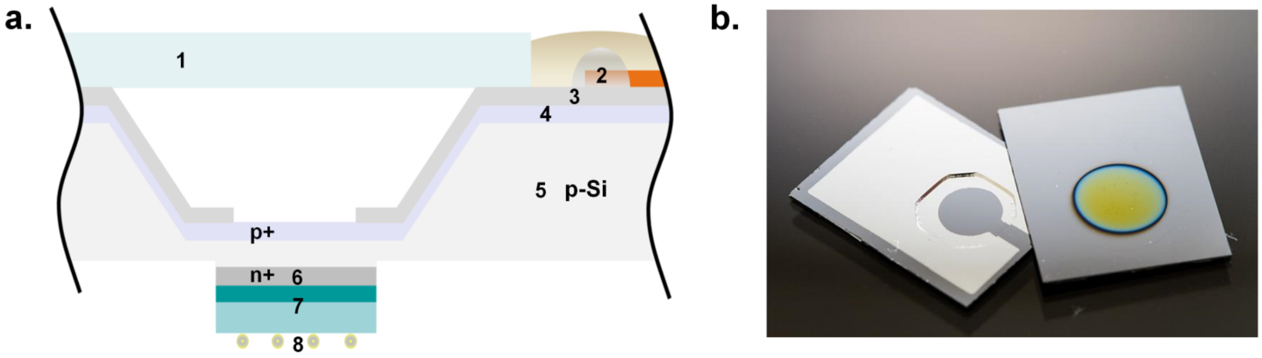

Figure S 2. Schematic cross section of multilayered-structure with classification numbers by its function (a), and optical image of cells used in this work (back-illuminated surface – left, front-illuminated surface – right). These samples were covered with Quartz glass and Teflon tape before the photochemical experiments.

Table S 1. Information of layers classified by its function in Figure S2.

№	Function	Material	Method
1	Cover window	Quartz glass	Epoxy bonding
2	Charge collector	Cu wire	Ag-paste
3	Back contact	Al	E-beam evaporator
4	Charge transfer (p^+) layer	Boron-doped Si	Ion-implantation
5	Light absorber (p)	p-type Si	(100) CZ wafer
6	pn-junction (n^+ layer)	Phosphorous-doped Si	Ion-implantation
7	Protection layer	TiO_2/Ti	DC sputtering with O_2 flow
8	Co-catalyst	Pt	Drop-casting (10 μL)

2. Structure and sample fabrication methods

ATiO$_2$/Ti layer was used as a corrosion protection layer at the semiconductor/liquid junction, and Pyrex glass cover as an isolation layer for the back-side to prevent from unexpected reaction. p^+ and n^+ doped layer were formed by doping with Boron and Phosphorous, respectively, using ion implantation, which was followed by annealing of the samples using rapid thermal process for distribution of implanted ions with minimized thermal redistribution of impurities at high temperature. The Al charge collecting layer was deposited by using the E-beam evaporation process. A circular hole for light incident in the middle of thinned surface was formed by using metallic shadow mask during the evaporation process. The depositedAlarea was turned into a fully connected area using Silver paint to leave a non-Al circular area with a diameter of 5 mm. The areas of these circular holeswere measured precisely by using image analysis program

ImageJ 1.46r. The front surfaces (bottom surface in Figure S2a) were covered by hole punched (Ø 5 mm) Teflon tape, and these holes were also measured precisely using the image analysis program. The Pt was drop-casted as a last step onto the opened TiO_2 surface.The detailed information of layers classified by its function can be found in Table S1.

3. Calculation for band diagram

3.1. Calculation at pn$^+$-junction

Most of this band diagram has already been demonstrated in our previous works1. In explaining the band diagram, we will start from the pn-junction of electrode and move towards the electrolyte. The p-Si wafer has a band gap (E_g) of 1.124 eV, an acceptor density (N_A) of $3 \cdot 10^{15}$ cm^{-3}. The bulk p-Si valence band (VB) can be determined as a function of working potential (E):

$$E_{V,\,p-Si} = E - \frac{kT}{e} ln\left(\frac{N_{A,p-Si}}{N_{V,\,Si}}\right)$$

In figure S3the working potential corresponds to the hole quasi-Fermi level. k is Boltzmann's constant, T is temperature (298 K), e is the elementary charge, and $N_{V,\,Si}$ is the density of states in the valence band, which is $1.8 \cdot 10^{19}$ cm^{-3} for Si2. Assuming the pinning of the band edges of the semiconductor at the interface (0 V vs. RHE) the $E_{V,\,p\text{-}Si}$is 0.22 V.

The Surface of the p-Si was doped with phosphorous by ion implantation process and n$^+$ emitter layer was formed at the surface. The process simulation program (Athena, SILVACO) was used to determine the donor density (N_D), which is approximately $5 \cdot 10^{19}$ cm^{-3}. The bulk valence band of the n$^+$ Si can be determined via equation:

$$E_{C,\,n-Si} = E + \frac{kT}{e} ln\left(\frac{N_{D,n-Si}}{N_{C,\,Si}}\right)$$

where N_C stands for the density of states in the conduction band, which is $2.8 \cdot 10^{19}$ cm^{-3} for Si2. Under the same assumption as above the $E_{C,n\text{-}Si}$ is 0.015 V.

At the pn$^+$-junction a built-in potential will be formed which can be determined in the dark via equation:

$$V_{bi} = \frac{kT}{e} Ln\left(\frac{N_{D,n-Si} \cdot N_{A,p-Si}}{n_i^2}\right)$$

where n_i is intrinsic carrier density of Si, which is approximately $1.5 \cdot 10^{10}$ cm^{-3} at room temperature, and V_{bi} was found to be 0.9 V. Under illumination V_{bi}at open circuit voltage conditions will simply be the V_{bi} in the dark minus the photo voltage (V_{ph}):

$$V_{bi,\,OCV} = V_{bi} - V_{ph}$$

If it is assumed that there are no interfacial losses at the pn$^+$-junction, the V_{bias} is distributed between the p-Si and n$^+$-Si as followed:

$$V_{bi,\,p-Si} = V_{bi,OCV}\frac{N_{D,n-Si}}{N_{A,p-Si} + N_{D,n-Si}}$$

$$V_{bi,n-Si} = V_{bi,OCV}\frac{N_{A,p-Si}}{N_{A,p-Si} + N_{D,n-Si}}$$

Using above equations, the $V_{bi,p\text{-}Si}$ is 0.43 V and $V_{bi,n\text{-}Si}$ is $1.3 \cdot 10^{-5}$ V.

The depletion width can be determined via equation:

$$W = \sqrt{\frac{2\varepsilon_0\varepsilon_{Si}\left(N_{D,n-Si} + N_{A,p-Si}\right)V_{bi}}{eN_{D,n-Si}N_{A,p-Si}}}$$

where ε_0 ($8.8 \cdot 10^{-12}$ F/m)3 is the permittivity in vacuum, and ε_{Si} is the relative permittivity of Si (11.7)4. From the equation mentioned above the sample was determined to have a depletion width of 640 nm. The depletion width is distributed between the p-Si and n$^+$-Si as followed:

$$x_p = \frac{N_{D,n-Si}}{N_{A,p-Si} + N_{D,n-Si}}W$$

$$x_n = \frac{N_{A,p-Si}}{N_{A,p-Si} + N_{D,n-Si}}W$$

From the equation above mentioned, most of depletion width will be in p-Si side and only 0.2 nm will be in n$^+$-Si layer.

3.2. Calculation at n$^+$-Si/Ti interface

In this work we assume the n$^+$-Si/Ti interface forms a Schottky barrier with no metal induced gap states or Fermi level pinning. If this is the case, the barrier height $\Phi_{B,Si}$ at the n$^+$-Si/Ti interface is the difference between the Ti work function (Φ_{Ti} = 4.33 V)5 and the n^+-Si ionization energy (Φ_{n+-Si}) plus the deviation between the flat band potential and the conduction band. Assuming that Φ_{n+-Si} is close to the electron affinity of Si (χ_{Si} = 4.15 V)6This is shown in equation below:

$$\Phi_{B,Si} = \Phi_{Ti} - \Phi_{Si} + \frac{kT}{e} ln\left(\frac{N_{C,Si}}{N_{D,n-Si}}\right)$$

$\Phi_{B,Si}$ was found to be 0.15 V. Since Ti is a metallic layer, and has a high carrier density compared to the Si, thus the bias will be distributed entirely over the n^+ Si region. The band bending distance in the n^+-Si can be determined by equation:

$$W_{n^+ Si/Ti} = \sqrt{\frac{2\varepsilon_{Si}\varepsilon_0\Phi_B}{eN_{D,n-Si}}}$$

The barrier width was found to be approximately 1.4 nm, and electron transfer from the Si to the Ti would most probably have to occur through tunneling.

3.3. Calculation at TiO_2/liquid interface

From the Mott-Schottky analysis the TiO_2 conduction band was determined to be -0.09 V vs. RHE, the donor density was $4.5\cdot10^{19}$ cm^{-3}, and the flat band potential was -0.07 V vs. RHE. Since the $E_{FB,\ TiO2}$ is very close to the work function of Ti, thus it can be assumed this junction will show Ohmic behavior. From our previous works we have seen that TiO_2-Pt system forms an Ohmic contact, thus there shouldn't be a barrier at the interface1.

The depletion region width of TiO_2 at the interface is given by:

$$W_{TiO_2/liquid} = \sqrt{\frac{2\varepsilon_o\varepsilon_{TiO2}\Phi_{B,TiO2}}{eN_{D,TiO_2}}}$$

ε_{TiO2} is the relative permittivity of TiO_2 (75)7, $N_{D,TiO2}$is the doping density of TiO_2 obtained from Mott-Shottky analysis ($4.5\cdot10^{19}$ cm^{-3}). $\Phi_{B,TiO2}$ is the barrier height at TiO_2/liquid interface, and it can be simply calculated by:

$$\Phi_{B,TiO_2} = E_{H^2/H_2} - E_{FB,TiO_2} + \frac{kT}{e} ln\left(\frac{N_{D,TiO_2}}{N_{C,TiO_2}}\right)$$

where $N_{C,TiO2}$ is the density of states in the conduction band, which is $6.8 \cdot 10^{20}$ cm^{-3} for $TiO_2$8. Since we assume that interface forms Fermi level pinning, above-mentioned equation results in $\Phi_{B,TiO2}$ of 0.038 V. Applying this values results in $W_{TiO2/liquid}$ of 1.02 nm.

3.4. Calculation at p^+p-junction

The shallow doped p^+-Si VB can be determined through the flat band:

$$E_{V,p^+-Si} = E - \frac{kT}{e} ln\left(\frac{N_{A,p^+-Si}}{N_{V,Si}}\right)$$

Using acceptor density values of p^+ Si $N_{A,p+-Si}$ ($1 \cdot 10^{20}$ cm^{-3}), the valence band of p^+ layer is 0.04 V. There are no simple expressions predicting the depletion width, but the width is on the order of a Debye length:

$$L_D = \sqrt{\frac{\varepsilon_0 \varepsilon_{Si} kT}{e^2 N_{A,p-Si}}}$$

Considering all values used above, the depletion width is approximately 75 nm.

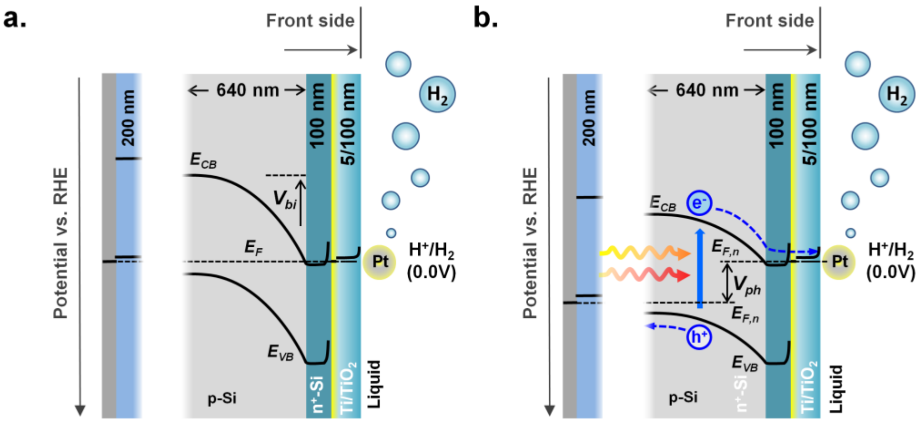

Figure S 3. Schematic energy diagram of the pn^+ Si with Ti-TiO_2 surface in the dark in equilibrium with the H^+/H_2 reaction (a), and illuminated condition with photovoltage (b).

Material and device parameters which have been used for the calculation also can be found in table S2:

Parameter	Definition	Value

$N_{A,\ p\text{-}Si}$	Acceptor density of p-Si	$3\cdot10^{15}$ cm^{-3} *
$N_{C,\ Si}$	Density of states of Si in conduction band	$2.8\cdot10^{15}$ cm^{-3}[2]
$N_{V,\ Si}$	Density of states of Si in valence band	$1.8\cdot10^{19}$ cm^{-3}[2]
$N_{D,\ n\text{-}Si}$	Donor density of n^{+}-Si	$5\cdot10^{19}$ cm^{-3} **
$N_{A,\ p+\text{-}Si}$	Acceptor density of p^{+}-Si	$1\cdot10^{20}$ cm^{-3} **
$N_{C,TiO2}$	Density of states of TiO_2 in conduction band	$6.8\cdot10^{20}$ cm^{-3}[8]
$N_{D,TiO2}$	Donor density of TiO2	$4.5\cdot10^{19}$ cm^{-3} ***
χ_{Si}	Electron affinity of Si	4.15 V [3]
Φ_{Ti}	Work function of Ti	4.33 [5]
ε_o	Permittivity in vacuum	$8.85\cdot10^{-12}$ F m^{-1} [3]
ε_{si}	Relative permittivity of Si	11.7 [4]
ε_{TiO2}	Relative permittivity of TiO_2	75 [7]

Table S2. Material and device parameters

*Provided by supplier (Topsil)

**Calculated using a process simulation program (Athena, SILVACO).

***Taken from the experimental Mott-Shottky analysis of TiO_2

4. Mott-Shottky analysis of TiO_2

To determine the TiO_2 conduction band, we provided Mott-Shottky analysis using 100 nm TiO_2/5 nm Ti deposited on n^{+} Si. The n^{+} Si was chosen to prevent unexpected photovoltage effect. This sample was tested electrochemically in 1 M $HClO_4$ electrolyte. For this experiment a modulation frequency of 10 kHz, perturbation amplitude of 35 mV has been used. Figure S4 shows the result of this experiment.

The flat band potential of TiO_2 can be estimated by using Mott-Shottky equation shown below:

$$\frac{1}{C^2}=\frac{2}{q\varepsilon_{TiO_2}\varepsilon_0 A N_{D,TiO_2}}\left(E-E_{FB}-\frac{kT}{e}\right)$$

where C is the measured differential capacitance per area. Using this equation results in a flat band potential of -0.07 V vs. RHE and dopant density of $4.5\cdot10^{19}$ cm^{-3}.

The conduction band can be found using the equation shown below:

$$E_C=E_{FB}-\frac{kT}{e}Ln\left(\frac{N_{D,TiO_2}}{N_{C,TiO_2}}\right)$$

The equation results in a conduction band at -0.09 V vs. RHE.

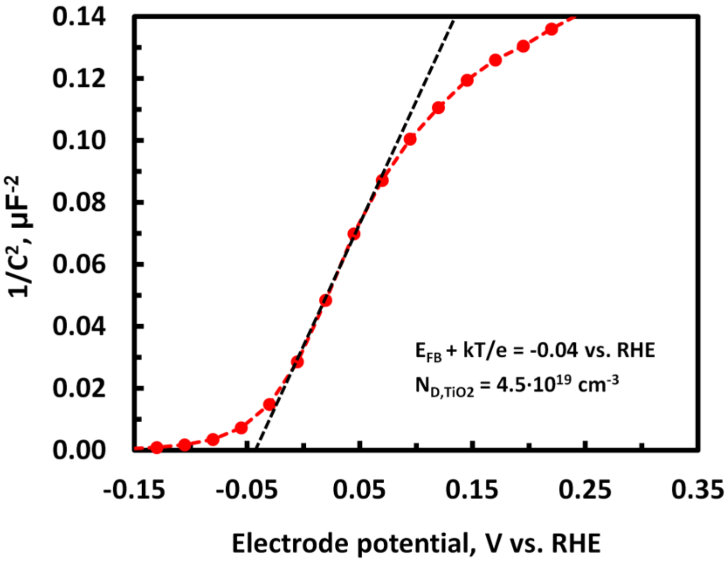

Figure S 4. Mott-Schottky plot of sputtered 100 nm TiO_2/5 nm Ti on n^+ Si surface.

5. Role of p^+ layer

Some samples were fabricated without p^+ doped layer to demonstrate the importance of having a p^+ sheet-conducting layer. The schematic cross sections of these samples can be found in Figure S5. All layers are fabricated using same process as mentioned in table S1. Figure S6 shows the cyclic voltammogram (CV) for photocatalytic H_2 evolution of the pn^+-Si electrodes with direct back contact at the middle of the sample and back contact on Al charge collector under front side illumination. H_2 could be visually observed bubbling off from the semiconductor/liquid interface as the current increased, and it was confirmed by GC measurement that hydrogen is produced with high Faradaic efficiency (Figure S9 in SI†). Both samples have open circuit voltage (V_{oc}) well in excess the H^+/H_2 redox potential (0 V vs. RHE).

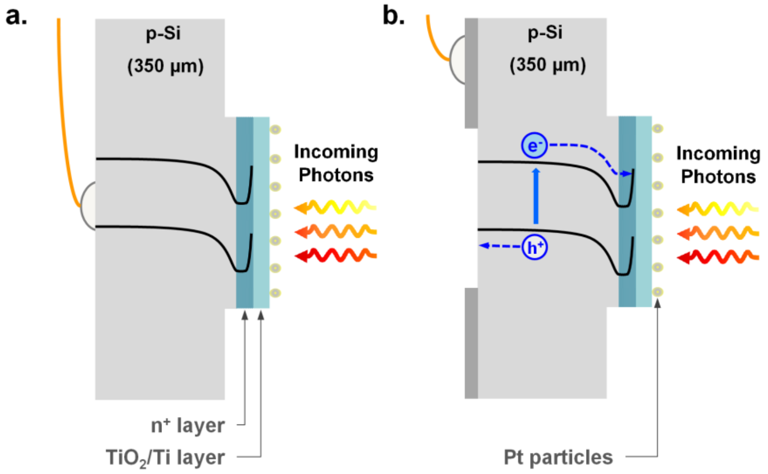

Figure S 5. Schematic cross section of front-illuminated samples of Figure S6. Cu-wire is directly connected on the back side (a) using Ga-In eutectic and Ag paste. Cu-wiring on Al layer (b) is also used to demonstrate the importance of having a sheet-conducting layer. These samples were covered with Teflon tape before the photochemical experiments.

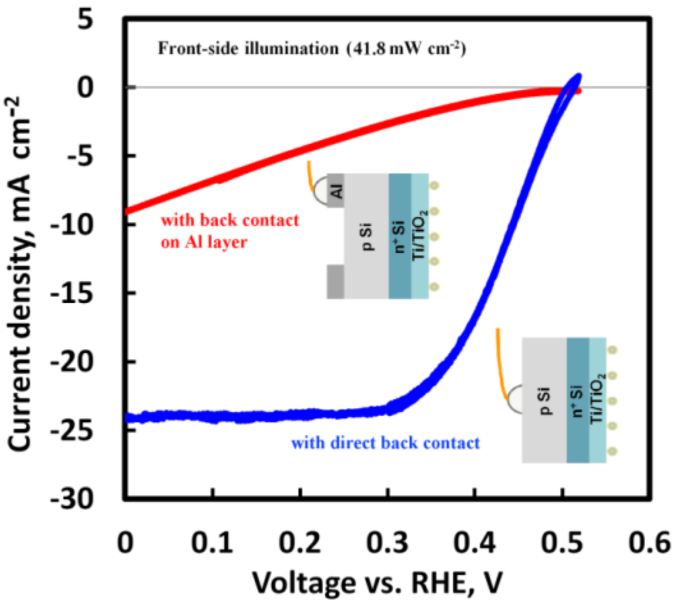

Figure S 6. CV of a pn$^+$-Si photocathode with direct back contact (blue) and one with back contact on Al charge collection layer (red) under front-illumination. This illustrates the severe series-resistance problem and thus the need for a transparent interlayer to form an efficient pathway for carriers.

The pn$^+$-Si with direct back contact has an onset of 0.49 V vs. RHE with J_L approximately 24 mA cm^{-2} under these conditions. On the other hand, the sample with an Al layer (red curve) back contact has a similar V_{oc}, but it has a very low J_L at 0 V vs. RHE due to a high series resistance. This shows that simply adding a ring-shaped Al charge collector layer is not sufficient to provide an efficient pathway for injected holes from Si. Thus there is a need for an additional transparent layer with low lateral resistance (R_l) in order to transfer the holes to the Al layer without significant Ohmic loss. Furthermore, since we wish to illuminate from the back, this transport layer must be transparent. This was achieved via a shallow boron doped p$^+$ layer, which is formed between the Al back contact and the p-Si substrate as shown in Figure 2a and b. This structure makes the overall series resistance of the device comparable to a conventional Si device with direct back contact. It was estimated that a doping concentration of 10^{20} cm^{-3} ($5\cdot10^{16}$ at/cm^2 at 100 keV) of boron could provide a sufficiently low sheet resistance to the Si surface9 and consequently an efficient carrier transport pathway.

8. Mathematical derivation of charge collection probability under back-illumination

Let us first consider a semiconductor slab of thickness L, with surface recombinationvelocity V_s at $z = L$, and diffusivity D for the minority carriers (electrons). We define the normalized surface recombination velocity as $S= V_s/D$. At $z = 0$ the excess electrondensity n_{e0} is assumed. The excess carrier density in steady state is governed by a continuity equation aforementioned in methods section. The solution of the equation is:

$$n_e = n_{e0}\frac{cosh\frac{L-z}{L_e} + SL_e sinh\frac{L-z}{L_e}}{cosh\frac{L}{L_e} + SL_e sinh\frac{L}{L_e}}$$

The electron flux density is then:

$$F =- D\nabla n_e = \frac{D}{L_e}n_{e0}\frac{sinh\frac{L-z}{L_e} + SL_e cosh\frac{L-z}{L_e}}{cosh\frac{L}{L_e} + SL_e sinh\frac{L}{L_e}}$$

Assume now electron hole pair generation at $z = z_0$ in a simple pn-junction model, where the total absorber thickness is L and the depletion layer has the boundaries at $z = z_b$ and $z = z_e$ while the back side at $z = 0$ has normalized recombination rate S. At the junction boundaries $n_{e0} = 0$ is assumed. The minority carrier electrons generated at z_0 will diffuse to the left and right and create the steady state excess carrier profile shown in Fig. S7; only the electron flux density at z_b contributes to the collected electrons. Thus the collection probability $C_P(z)$ is the flux density at

z_b divided by the sum of flux density magnitudes at z_0. The flux densities magnitudes can be written as follows:

$$F(z_b) = \frac{D}{L_e} n_{e,\, z_0} \frac{1}{\sinh \frac{z_b - z_0}{L_e}},\ Note\ S \rightarrow \infty\ at\ z = z_b;$$

$$F(z_0)_{right} = \frac{D}{L_e} n_{e,\, z_0} \frac{\cosh \frac{z_b - z_0}{L_e}}{\sinh \frac{z_b - z_0}{L_e}};$$

$$F(z_0)_{left} = \frac{D}{L_e} n_{e,\, z_0} \frac{\sinh \frac{z_0}{L_e} + SL_e \cosh \frac{z_0}{L_e}}{\cosh \frac{z_0}{L_e} + SL_e \sinh \frac{z_0}{L_e}}$$

and thus the collection probability becomes:

$$C_P(z) = \frac{F(z_b)}{F(z_0)_{right} + F(z_0)_{left}} = \frac{1}{\cosh \frac{z_b - z_0}{L_e} + \sinh \frac{z_0}{L_e} \cdot \frac{\sinh \frac{z_0}{L_e} + SL_e \cosh \frac{z_0}{L_e}}{\cosh \frac{z_0}{L_e} + SL_e \sinh \frac{z_0}{L_e}}}$$

In the depletion layer the $C_P(z)$ is 1. As already shown in our previous work[3], the depletion layer of our pn$^+$ Si is approximately 640 nm, but its contribution under the back-illumination is negligibly small since the normalized charge generation rate $G(z)$ is close to zero at the junction boundary.

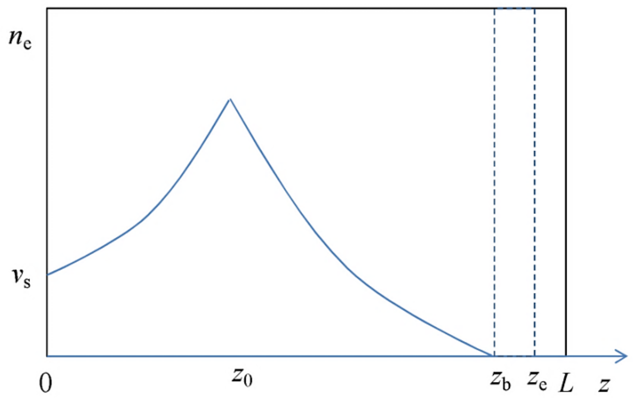

Figure S 7. Simple photoabsorber model with pn-junction. The blue curve illustrates how electron density changes with depth in photoabsorber when the electron-hole pair generation occurs at point z_0.

6. Absorption properties of silicon

The optical properties of silicon were measured at 300K[10]. The absorption length (δ_p) is the inverse of the absorption coefficient (α). The index of refraction (n) for silicon is also plotted. These n and α were used in this work for determination of absorbance (a) by using Equation 6 in main manuscript.

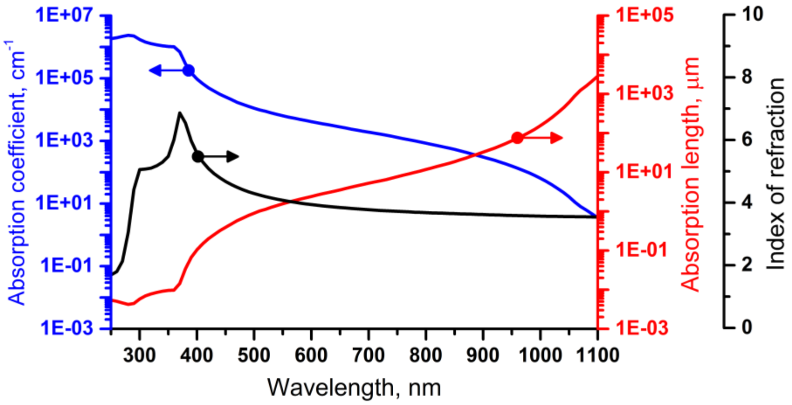

Figure S 8. Absorption coefficient of silicon in cm^{-1} as a function of the wavelength (blue) and absorption length in silicon (red). Silicon is an indirect band gap semiconductor so there is a long tail in absorption out to long wavelengths. The data is graphed on a log scale, and the drop in absorption at the band gap (around 1100 nm) is sharper than might first appear. The n value, *i.e.* index of refraction, of silicon is also plotted (black).

7. H_2 quantification method

H_2 quantification was carried out using a gas chromatograph (Hewlett Packard 5890 Series II) equipped with a Molsieve-5A PLOT column (carrier gas: Ar), a thermal conductivity detector and automated gas sampling. A diaphragm pump (KNF, NF5RPDCB-4) was used to keep the gas in the working electrode compartment flowing through the gas chromatograph (GC) closed sample loop and bubbling through the electrolyte. Before the reactions, both the counter and the working electrode compartments were flushed with Ar gas and the cell was closed off. The headspace gas composition of the working electrode was sampled every 10 minutes throughout the entire length of the experiments (as the red dots in the plot below). A pure Pt wire was used as a standard to calibrate the H_2 signal before the experiment using the same GC. The number of moles of H_2, n_{H2}, was then extracted using the ideal gas law. Finally, the corresponding charge, Q_{H2}, was obtained via the equation $Q_{H2}= 2Fn_{H2}$, where F is the Faraday constant. In Figure S9, fluctuation of the photocurrent in the first 30 min is shown, and then stabilizes. This might be due to the unstable light irradiation. The evolved H_2 as measured by GC of the head space is represented by red dots. The measured amount of H_2 closely matches the expected amount of H_2 which is calculated taking into account the amount of charge passed through the circuit (black dashed line). This demonstrates that the current is indeed due to photocatalytic hydrogen evolution close to unity Faraday efficiency.

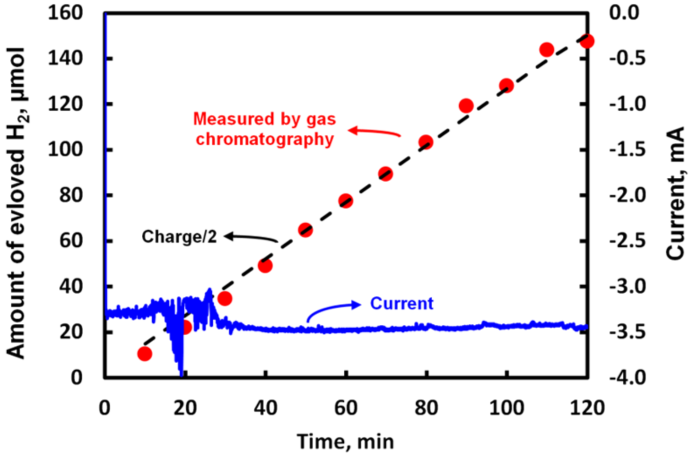

Figure S 9. Hydrogen evolution as a function of time measured with a gas chromatograph and corresponding current over the back-illuminated Pt/TiO_2/Ti/p^+pn^+ Si at 0 V vs. RHE. The illuminated area is 0.201 cm^2 and the sample is under red-light irradiation (Xe lamp with AM 1.5 and 635-nm-cut-off filters). The current initially decays 5% in the first 30 min and then stabilizes.

9. Thickness effect on IPCE

The slops and intensities ofincident photon to current efficiency (IPCE)decrease with the thickness of Si under back illumination. This is highly related with L_e/L decrease effect on the charge collection probability as shown in Figure 7 in main manuscript. On the other hand, IPCE under the front-illumination showed gradual decrease only in long wavelength range with decrease of Si thickness. Since photons with longer wavelengths penetrate deeper into the silicon, under back-illumination electron-hole pairs generated from longer wavelength photons are therefore generated closer to the pn$^+$-junction boundary under back-illumination. However, in the front illuminated case most of carriers are generated close to the pn$^+$-junction regardless of the Si thickness.

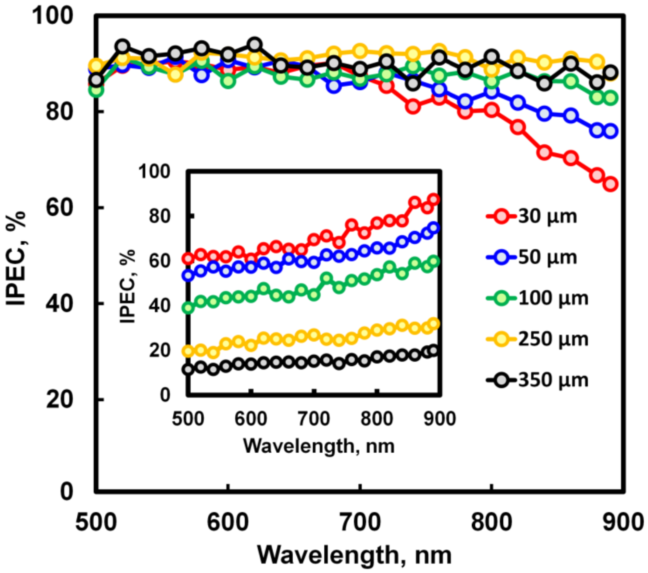

Figure S 10.IPCEfrom the Si photocathodes with various thicknesses under front and the back-illumination (inset). The slop and intensity of IPCE increase gradually with decrease of Si thickness under the back-illumination, whereas for the front-illuminated case intensity decreases slightly with decrease of the thickness only in the long wavelength range.

10. Reflectance and transmittance measurement

Reflectance from the back side (Quartz/air/SiO_2/Si side) and front side (TiO_2/Ti/Si) was measured by using an integrating sphere (Mikropack ISP-50-8-R-GT). As shown in Figure S11 the reflectance of the back side exceeds 16% over the full spectral range, whereas reflectance from the front side (TiO_2/Ti/Si) was less than 10% at wavelengths $\geq$ 635 nm. It seems that the high reflectivity of the back side contributed to the low IPCE at longer wavelengths under the back-illumination. Also, the high IPCE over 90% under front-illumination might be due to this anti-reflective property of the TiO_2 protection layer.

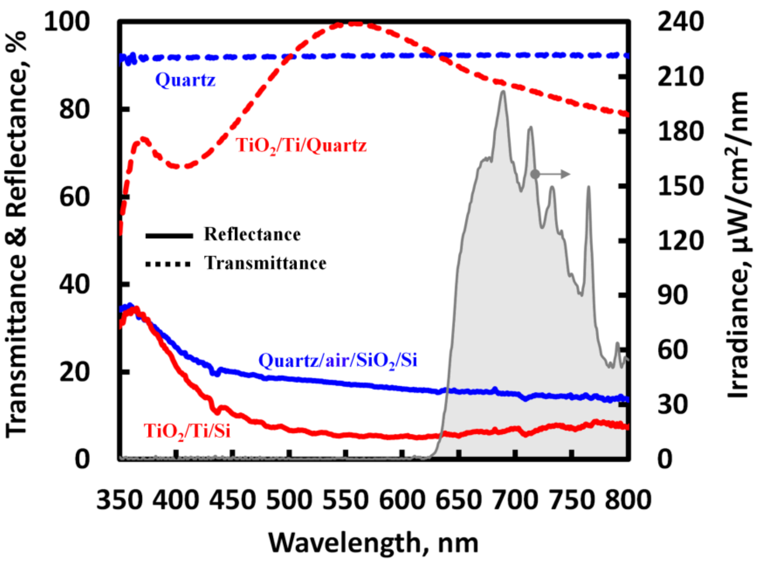

Figure S 11. Reflectance of Quartz/air/SiO_2/Si and TiO_2/Ti/Si are given (solid) with the transmittance of 500-μm-thick Pyrex and 100-nm-thick TiO_2 which are used as a cover glass for the back-side and a protection layer for the front-side, respectively (dot). Irradiance of the light from the solar simulator used in this work is also given.

11. IPCE & APCE vs. $C_P(z)$

The measured IPCE corresponds to incident photon to current efficiency ratio, and it is the ratio of the number of charge carriers collected by the device to the number of photons of a given energy shining on the device from outside (incident photons). To estimate more precise charge collection behavior, we have calculated theabsorbed photon to current efficiency ratio (APCE), which is the ratio of the number of charge carriers collected by the device to the number of photons of a given energy that are absorbed by the device. The APCE can be calculated from ICPE by using following relationship:

$$APCE = \frac{IPCE}{1 - R - T}$$

where R is the reflectance and T the transmittance of the sample. The measured reflectance data in Figure S11 were used in this equation. As shown in Figure S12, the APCE in term of absorption depth of the light in Si shows a behavior quite similar to calculated $C_P(z)$ with L_e = 400 μm and S = 170 cm^{-1}. (Note: for APCE the transmittance of the Si wafer was not taken into account).

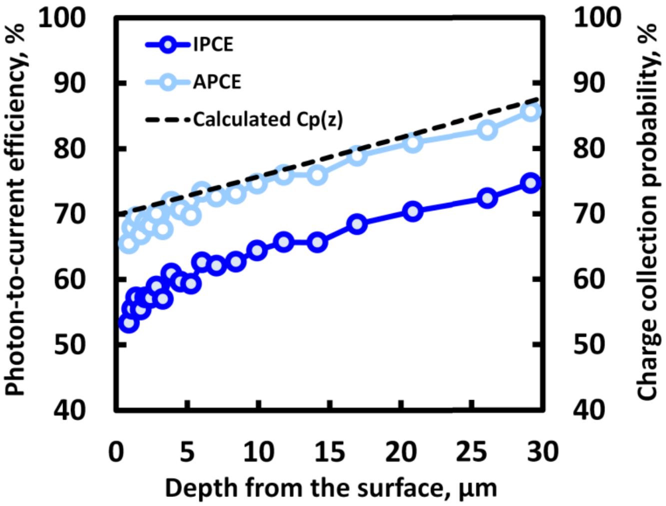

Figure S 12. Incident photon to current efficiency (IPCE, dark blue) and Absorbed photon to current efficiency (APCE, light blue), which was converted from IPCE considering the reflectance of back side. Calculated $C_P(z)$ is also shown to compare with APCE.

12. Thickness effect on CV under back-illumination

Photocurrent of Si photocathode increases under back-illumination along with the decrease of the thickness. 50-µm-thick Sample showed highest current density over 17 mA cm^{-2}. However 30-µm-thick sample is outperformed by the 50-µm-thick sample indicating that absorption losses at long wavelength start to dominate the charge collection losses.

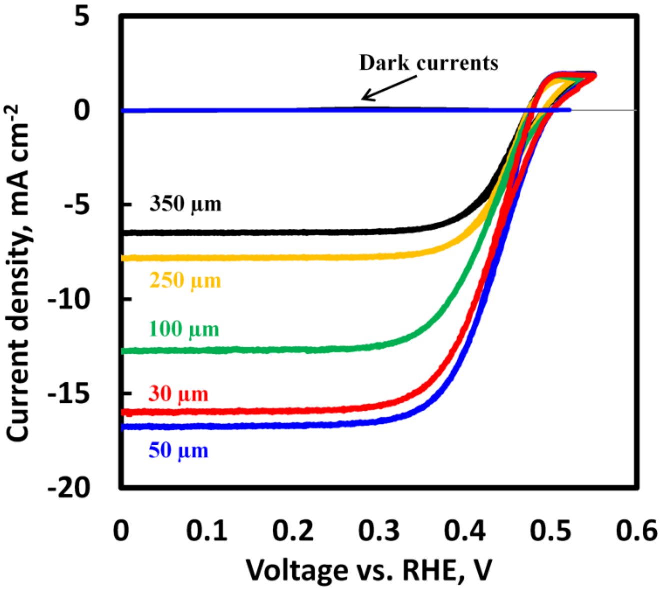

Figure S 13.CVs of Si photocathodes with various thicknesses. The total irradiance is 41.8 mW cm^{-2}. Assuming that S and L_e of all samples is same, this shows how L_e/L affects J_L of the device.

1. B. Seger, T. Pedersen, A. B. Laursen, P. C. K. Vesborg, O. Hansen, I. Chorkendorff, *Using TiO_2 as a conductive protective layer for photocathodic H_2 evolution*, J. Am. Chem. Soc., 2013, **135**, 1057−1064.
2. L. Vivien, L. Pavesi, *Handbook of silicon photonics*, Taylor & Francis, Boca Raton, 2013, ch. 1.3., p. 26.
3. The NIST reference on constants, units, and uncertainty, http://physics.nist.gov/cgi-bin/cuu/Value?ep0 (accessed Nov. 24, 2014).
4. M. –K. Lee, H. –C. Lee, C. –M. Hsu, *High dielectric constant titanium oxide grown on amorphous silicon by metal-organic chemical vapour deposition*, *Semicond. Sci. Technol.,* 2006, **21,** 604-607.
5. H. P. R. Frederikse, CRC Handbook of Chemistry and physics, ed. by D. R. Lide, 78th edition, 1997, pp 12.
6. N. Dasgupta, A. Dasgupta, *Semiconductor devices: modeling and technology*, Prentice-Hall, New Delhi, 2004, ch. 1.3.10., pp. 30.
7. D. M. King, X. Du, A. S. Cavanagh, A. Weimer, *Confinement in amorphous TiO_2 films studied using atomic layer deposition*, Nanotechnology, 2008, **19**, 445401-445406.
8. J. Bisquert, A. Zaban, M. Greenshtein, I. Mora-Sero, *Determination of rate constants for charge transfer and the distribution of semiconductor and electrolyte electronic energy levels in dye-sensitized solar cells by open-circuit photovoltage decay method*, J. Am. Chem. Soc., 2004, **126**, 13550-13559.
9. W. R. Thurber, R. L. Mattis, Y. M. Liu, J. J. Filliben, *Resistivity-dopant density relationship for boron-doped silicon*, J. Electrochem. Soc., 1980, **127**, 2291-2294.
10. M. A. Green, M. J. Keevers, *Optical properties of intrinsic silicon at 300 K*, Prog. Photovoltaics, 1995, **3**, 189-192.